scientific reports

Check for updates

OPEN

Highly efficient electrochemical biosensing platform in breast cancer detection based on MOF-COF@Au core-shell like nanostructure

Ehsan Dezhakam[1,2], Roya Faraghi Vayghan[1], Sarina Dehghani[1], Taha Kafili-Hajlari[1], Abdolhossein Naseri[1,3]✉, Mehdi Dadashpour[2,4,5]✉, Balal Khalilzadeh[6,7]✉ & Gulsah Saydan Kanberoglu[8]

Nowadays, rapid and facile diagnosis of cancer using user friendly processes has attracted much attention. In this regard, an electrochemical (EC) biosensor with high sensitivity was fabricated by merging MIL156 MOF@COF nanocomposite with Au nanoparticles for the detection of CA15-3. Herein, metal clusters of MIL-156 as a Metal organic frameworks (MOF) were coated by a crystalline covalent organic frameworks (COF) through covalent bonding and created core-shell-like structures. The active part of the working electrode was modified in two consecutive steps. First, MIL-156 MOF@ COF and then Au nanoparticles were electrodeposited on the glassy carbon electrode (GCE). The porosity of nanocomposite has significantly increased the surface area and improved the conductivity. Au nanoparticles also form an acceptable substrate for bonding antibodies due to their high affinity with amino groups. In addition, Au nanoparticles amplify the EC signal of the biosensor with their undeniable conductivity. Nanocomposite was characterized with XRD, SEM, and EDAX techniques. To investigate the proposed biosensor, differential pulse voltammetry (DPV) was used as an analytical technique. The CA15-3 calibration provided a linear range between concentrations of 30 and 100 nU/ mL, thus expressing the powerful diagnostic potential of the designed biosensor. Furthermore, the suggested biosensor has been used in serum samples and discriminate breast cancer sufferers from healthy individuals with high confidence levels.

Keywords MIL-156 MOF, COF, Electrochemical Biosensor, Breast cancer, CA15-3

Cancer is one of the diseases that grow uncontrollably in tissues and tumor cells can spread to other organs through body fluids such as blood, urine, and mucus[1]. Breast cancer remains the most prevalent diagnosed cancer and 2nd leading cause of cancer mortality in women worldwide[2]. About 10% of breast cancer patients have a hereditary cause[3]. Reliable biomarkers for early diagnosis, tracking treatment response, and monitoring relapse are critically needed to guide clinical management and improve patient outcomes[4]. CA15-3 is a mucin-1 protein highly expressed in breast cancer that has emerged as the most widely used circulating biomarker in metastatic disease[5]. The prevalent diagnosis of breast cancer essentially depends on various clinical tools, including ultrasound, X-ray, mammography, histopathology, and magnetic resonance imaging (MRI)[6]. MRI is one of the sensitive techniques to detect breast cancer, but it is not economical and time-consuming. Histopathology requires

[1]Department of Analytical Chemistry, Faculty of Chemistry, University of Tabriz, Tabriz, Iran. [2]Department of Medical Biotechnology, Faculty of Medicine, Semnan University of Medical Sciences, Semnan, Iran. [3]Chemistry and Chemical Engineering departmen, Khazar University, 41 Mehseti Street, Baku AZ1096, Azerbaijan. [4]Cancer Research Center, Semnan University of Medical Sciences, Semnan, Iran. [5]Student Research Committee, Semnan University of Medical Sciences, Semnan, Iran. [6]Stem Cell Research Center, Tabriz University of Medical Sciences, Tabriz, Iran. [7]Hematology and Oncology Research Center, Tabriz University of Medical Sciences, Tabriz, Iran. [8]Department of Chemistry, Faculty of Science, Yuzuncu Yil University, Van 65080, Turkey. ✉email: ab.naseri@gmail.com; dadashpourmehdi1400@gmail.com; balalkhalilzadeh@gmail.com; khalilzadehb@tbzmed.ac.ir

living tissue for diagnosis, which makes it an invasive method. X-ray and mammography provide appropriate diagnoses, but repeated or prolonged exposure to dangerous radiation may eventually increase the threat of malignancy[7]. Clinical methods require a long time to detect cancer metastasis, which causes low sensitivity and accuracy[8]. Considering the mentioned limitations, the development of non-invasive, low-risk, rapid, cost and time-effective, and sensitive methods for breast cancer diagnosis is urgent. Here, various approaches have been extended for probe molecule evaluation, such as fluorescence assays[9], enzyme-linked immunosorbent assays (ELISA)[10], electrochemical (EC) methods[11], electrochemiluminescence (ECL)[12], and colorimetric assays[13].

Biosensors consist of a receiver and a transducer, which connect the biological agent and the substrate and convert their effect into a measurable signal[14,15]. EC biosensors have many advantages that make them superior to other techniques, such as easy and fast operation, cost-effectiveness, high specificity, selectivity, and sensitivity[16]. One of the reasons for using EC biosensors in point-of-care testing (POCT) is their rapidness and the availability of portable devices[17]. Another obvious motive is their non-invasiveness, which prevents possible side effects[18]. In addition, they are used in various fields, such as the food industry, pharmacology, and medicine[19,20]. It is noteworthy that early detection of cancer is an essential factor in the treatment process[14,21,22]. Immunosensors are a subgroup of biosensors whose main recognition element is an antibody. Antibodies have a protein structure that is produced by living tissue in the versus of an external stimulus. Immunosensors have good stability and are specific for antibodies[23,24]. Using nanomaterials improves the effective surface area of biosensors and provides a suitable platform for immobilizing different biological agents[25–27]. The immobilizing of nanomaterials on the electrode active part speeds up electron transfer and makes the EC biosensor more stable by preserving the antibody during the analysis conditions[28]. EC biosensors can detect multiple analytes simultaneously. These undeniable advances in biosensing are promising for the early diagnosis of diseases[29]. Recently, the application of porous materials for molecular surface tuning has been very concerning. Metal-organic frameworks (MOFs) and covalent organic frameworks (COFs) are two classes of porous materials that have attracted the interest of researchers. MOFs and COFs can substantially enhance the response of EC biosensors compared to other traditional materials[30,31]. MOFs are compounds containing multi-node metal clusters and organic ligands[32]. They have a high surface area, tunable pores, and good electronic transferring ability[33]. Thus, MOFs have been exploited in chemical and biological sensors, catalytic activities, biomedicine, etc[34,35]. COFs are materials with two- or three-dimensional structures that are constructed from molecular units connected by strong covalent bonds[36]. COFs are usually used in various fields due to their advantages, including good stability, regular pores, low density, biocompatibility, and large surface area[37–39]. According to the present information, COFs and MOFs have the desirable potential to provide a suitable substrate for the immobilization of antibodies and improve the performance of the biosensors. In addition, Au nanoparticles, by anchoring through the link between Au-S and Au-NH_2groups, create a regular molecular connection, and due to their excellent conductivity, they significantly increase the electrical current. Hence, they are a favorable choice for use in biosensing methods[25,40]. MIL-156 MOF@COF as electrode surface modifier, which includes both MOF and COF structure. This nanocomposite has a core-shell like structure, where MIL-156 acts as the MOF, which is like the core part, and the COF forms the shell part. Due to its crystalline structure and regular pores, the COF can increase the surface area and the MOF can improve the conductivity; both of them increase the efficiency of the designed EC biosensor and make it possible to reach a lower detection limit, or, in other words, increase the sensitivity of the EC biosensor[41,42]. In this study, an EC immunosensor was prepared using MIL-156 MOF, which was decorated with COF, for the evaluation of breast cancer cells. Furthermore, the fabricated device was applied to distinguish between normal and breast cancer patients using the protein content of the breast cancer cell marker (Fig. 1).

Experimental

Materials

Gallic acid monohydrate ($C_7H_6O_5.H_2O$) (Sigma Aldrich), KOH pellets (Alfa Aesar), Tb (1,3,5-triformylbenzene) (J&K Chemical Ltd), Bd (benzidine), (Aladdin Chemistry), DMSO, DMF, calcium hydroxide $Ca(OH)_2$ (Aldrich), acetic acid, THF, ethanol, nitric acid, potassium hexacyanoferrate ($[Fe(CN)_6]^{3-/4-}$), PBS (pH = 7.4) were used in analytical grade without any purification. Tetrachloroauric (III) acid trihydrate ($HAuCl_4.3H_2O$), potassium chloride (KCl), sulfuric acid (H_2SO_4), hydrochloric acid (HCl, %37 wt), alumina powder (Al_2O_3), terephthalic dialdehyde ($C_6H_4(CHO)_2$), benzidine ($(C_6H_4NH_2)_2$) and potassium hexacyanoferrate ($K[Fe(CN)_6^{3-/4-}]$), were obtained from Merck. Phosphate-buffered saline (PBS) with a pH of 7.4 was prepared using KCl (0.2 g), NaCl (8 g), Na_2HPO_4 (1.44 g), and NaH_2PO_4 (0.24 g), dissolved in about 800 mL of distilled water, which all purchased from Merck. CA15-3 biotinylated monoclonal antibody, CA15-3 antigen, and the human serum samples were sourced from Imam Reza hospital.

Apparatus

All EC processes were measured by a RadStat-10 potentiostat/galvanostat EC analyzer (Kianshardanesh, Iran). A three-electrode system was used for analytical recording, including a GCE as the working electrode, an Ag/AgCl electrode as the reference electrode, and a platinum wire as the counter electrode. The whole procedure of preparation and analysis was performed in the laboratory ambiance. The suspensions were uniformly homogenized with a magnetic stirrer (Heidolph) and an ultrasonic device (Strasonic 35). The presence of constituent elements and SEM images were obtained by the Tescan instrument (model: MIRA3).

Synthesis of MIL-156 MOF

For the synthesis of MIL-156 MOF, $[Ca_3K_2(H_2O)_2(gal)_2].\ nH_2O$ ($n = 4–6$), gallic acid monohydrate (188 mg, 0.001 mol) was added to 10 mL of ultrapure water at 25 °C. Next, $Ca(OH)_2$(74 mg, 0.001 mol) was dissolved in the prepared solution. Following, the KOH 5 M solution was slowly added until the pH of the solution became alkaline (~ 800 mL = ~ 0.004 mol). Then, the prepared mixture was placed in a hydrothermal autoclave, heated

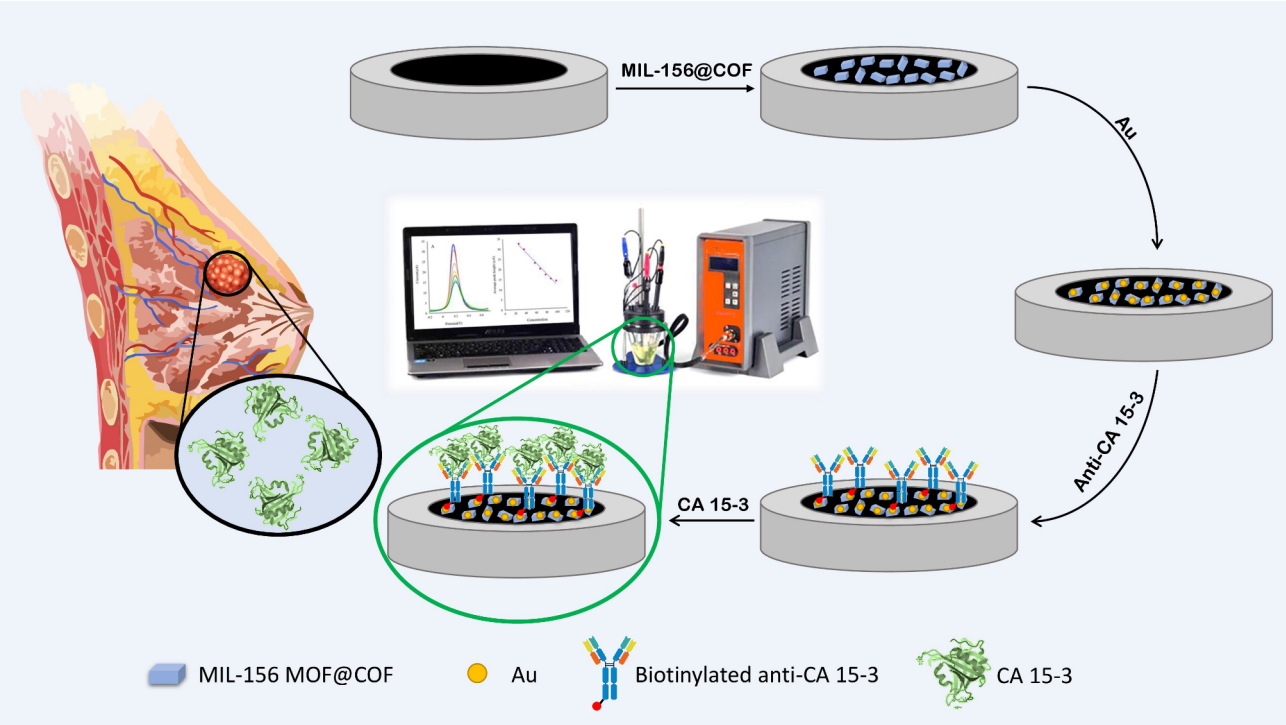

Fig. 1. Schematically presentation of developed immunosensor.

to 120 °C for 60 min, and kept under these conditions for one day. The obtained product, which was cooled to 25 °C after passing through the filter, was washed several times with double-distilled water and left to dry until the formation of MOF crystals[41].

Synthesis of COF (Fe3O4@PDA@TbBd)

According to previous reports, Fe_3O_4@PDA nanospheres were prepared[43]. In brief, Tb and Bd, 0.3 and 0.45 mmol, were added to DMSO (50 ml), respectively. Then, 0.15 g of Fe_3O_4@PDA was added to the above mixture, and the resulting suspension was ultrasonicated for 5 min. After that, 2 mL of HOAc was trickled slowly and kept still for 15 min at 25 °C until the reaction was carried out. Next, the obtained precipitate was washed continuously with pure ethanol and tetrahydrofuran. Eventually, the prepared COF dried in vacuum conditions at room temperature[44,45].

Synthesis of MIL-156 MOF@COF

The synthesis of MIL-156 MOF@COF starts by pouring 0.2 g of the MIL-156 MOF prepared from the above steps into 20 mL of DMF solution. Next, 0.4 and 0.55 g of terephthalic dialdehyde and benzidine were added to the desired mixture, respectively. To distribute the particles homogeneously, the mixture was sonicated for 5 to 10 min. Then 2 ml of acetic acid was added to the mixture and stirred slowly. Finally, the filtered MIL-156 MOF@COF was dried at 50 °C.

Preparation of MIL-156 MOF@COF suspension

To prepare 3 mg/mL of MIL-156 MOF@COF suspension, 0.03 g of MOF@COF was poured in 10 mL of distilled water (DW) and sonicated for 2 h. Next, 2 mL of the homogeneous mixture was appended to 8 mL of 0.1 M KCl solution.

Preparation of AuNPs solution

A solution of AuNPs with a concentration of 1 mM was prepared by mixing 7.876 mg of $HAuCl_4.3H_2O$ with 550 µL of 0.5 M H_2SO_4, followed by the addition of 20 mL of distilled water.

CA15-3 immunosensor fabrication

Information on the work steps: Briefly, to clean the electrode surface, the glassy carbon electrode was polished using alumina powder and a polishing pad. Then the electrode was washed with DW. After that, the chronoamperometry (CHA) technique was used to modify the electrode surface with MIL-156 MOF@COF by applying a potential of -3 V for 60 s. Stable readout signals are generated by the desirable electrodeposition of nanoparticles on the electrode surface. For this purpose, the Au nanoparticles were immobilized on the modified electrode via the CHA technique (-1 V, 30s) to create an appropriate substrate for anchoring the antibody and improving the conductivity. Afterward, the antibody was diluted with PBS (pH = 7.4) to 0.01 µg/mL, and 5 µL of the CA15-3 antibody was cast on the final modified electrode and stored for half an hour at 4 °C. Then, two

microliters of antigen CA15-3 with a certain concentration were dropped on the electrode and incubated for another half an hour at 4 °C. Non-adherent particles were washed with DW at the end of each incubation step to avoid disruption.

Results and discussion

Characterization of materials

The morphology of the fabricated biosensor has been tested by scanning electron microscopy (SEM), and energy dispersive X-ray analysis (EDAX). Figure 2 illustrated the representative SEM images with bare, MIL-156 MOF@COF-GCE, and Au-MIL-156 MOF@COF-GCE. As shown, two distinct substrates in terms of morphology and structure justify the proper modification of the electrode by nanocomposites (Fig. 2- **A and D**). Spheres with good dispersion on porous surfaces represent modifier electrodeposits with a diameter of about 209.91 nm. The existing porosity increases the surface area making it a desirable base for the electrodeposition of Au nanoparticles in the next stage of electrode modification. Based on dot mapping analysis, C and O elements form the main skeleton. Furthermore, Ca, K, and Au elements have also been observed, which justifies the existence of Ca and K in the structure of MOF, and the high percentage of Au element reveals its extraordinary loading (Fig. 2- **H**). The weight% of each element is presented in **Table S1**. The X-ray diffraction (XRD) pattern related to the nanocomposite is shown in the Fig. 3. Peaks at 20.26° and 23.92° are related to COF and the diffraction peak observed at 28.96°belongs to MOF crystal plates[41,46,47].

Optimization of electrodeposition potential of MIL-156 MOF@COF

For the electrodeposition of MIL-156 MOF@COF on the GCE, the CHA technique was used. In this regard, some experimental conditions were optimized, like electrodeposition potential and time. Thus, several potentials (0, 1, -3.5, -3.3, -3.1, -3, -2.9, and − 2.7 V) were utilized at a fixed deposition time (60 s), and each of them was studied in 0.005 M $[Fe(CN)_6]^{3-/4-}$/100 mM KCl solution[34]. As shown in Fig. 4A, when the potential decreases, the output current signal is strongly decreasing, and with increasing the value of potential, the current gradually increases so that the maximum amount of current is observed at -3 V. It is noteworthy that the excessive increase in potential causes the accumulation and oversaturation of MOF@COF nanocomposite on the electrode, as a result of which the conductivity and subsequently the efficiency of the EC biosensor decreases[48]. Based on this, -3 V was chosen for optimal potential.

Optimization of electrodeposition time of MIL-156 MOF@COF

According to the above description, we also optimized the electrodeposition time of MIL-156 MOF@COF. For this purpose, we checked different times (15, 30, 45, 60, 90, 120, and 240 s) and performed the same manner as mentioned in the potential optimization and investigated in 0.005 M of $[Fe(CN)_6]^{3-/4-}$/100 mM KCl solution. As time decreases, the nanocomposite does not entirely cover the electrode surface. As a result, the output signal decreases, and as time increases, more MOF@COF particles are placed on the surface, causing the appearance of massive currents (Fig. 4B). The excessive accumulation of nanocomposite, which occurs with increasing electrodeposition time, disrupts the electroactive molecules and reduces the performance of the EC biosensor. According to the results, the 60 s was chosen as the optimal time.

Optimization of electrodeposition potential of Au-MIL-156 MOF@COF-GCE

As mentioned before, Au particles are the interface between nanocomposite and biological molecules through the bonding between Au-S and Au-amine groups, and they affect the response of EC biosensors and their stability. For the desirable performance of Au particles, the electrodeposition process was studied. In this regard, several potentials (-0.75, -0.8, -0.9, -1, -1.1, -1.25, and − 1.5 V) were investigated and analyzed in a similar experimental ambiance (0.005 M $[Fe(CN)_6]^{3-/4-}$/100 mM KCl solution). The obtained results show that with increasing potential up to -1 V, the output currents also increase due to the significant conductivity of Au particles. An extra increase in electrodeposition potential causes excessive condensation of Au particles on the nanocomposite and saturates its surface, thereby making its performance negative. Consequentially, -1 V was used as the optimal potential for the electrodeposition of Au particles (Fig. 4C).

Optimizing the electrodeposition time of MIL-156 MOF@COF@Au

The next step in Au particles optimization is time optimization. To this end, six different times (15, 20, 30, 45, 60, and 180 s) were carried out using the optimal electrodeposition potential (-1 V) and examined in 0.005 M $[F(CN)_6]^{3-/4-}$/100 mM KCl solution. According to Fig. 4D, the short times for immobilizing Au particles on the MOF@COF-GCE are not enough, and the related signals were unfavorable. On the other hand, if the selected electrodeposition time is too long, the surface becomes saturated, and the performance of MOF@COF will be disturbed. In 30 s, the loading amount of Au particles was acceptable, and a high current appeared, which makes the 30 s the optimal time.

Electrode preparation steps

CV, EIS, DPV and SWV were the 4 methods used to analyze the prepared EC biosensor. As shown in Fig. 5, with the electrodeposition of the MOF@COF on the bare GCE, the received signal increased significantly. With the electrodeposition of AuNPs in the next step, the current continued to increase. These results are due to the suitable coating of MOF@COF on the electrode surface and also using Au to improve the conductivity. After modification of the electrode to enhance the surface of the electrode and increase the stability of currents, breast cancer specific antibody and antigen are loaded on the modified electrode. 6-Mercapto-1-hexanol (MCH) was used as a blocking agent after the antibody immobilization step, but according to **Fig. S3**, there was no significant change in the output signals, which shows that the surface is significantly covered by the antibody. Figure 5

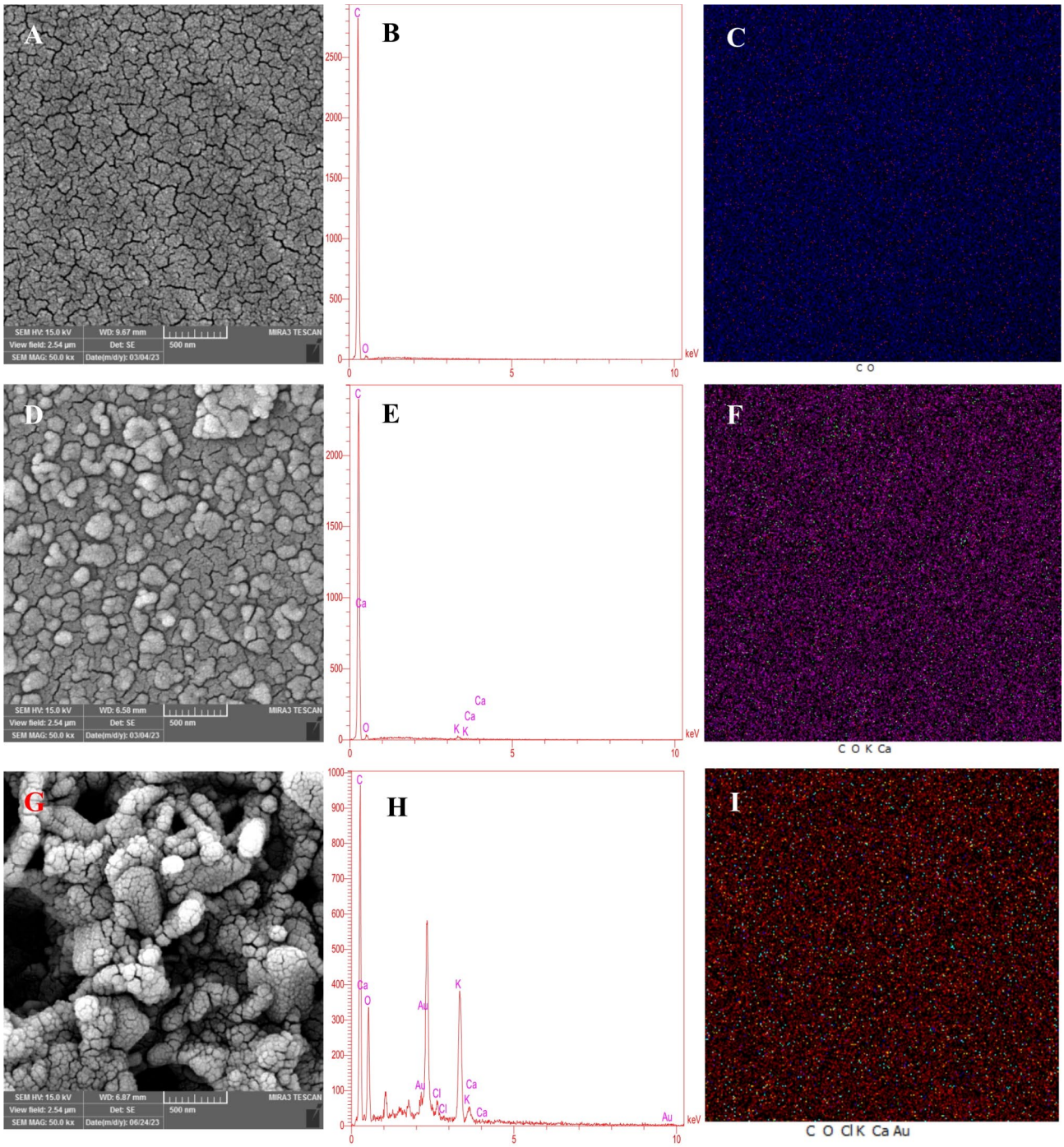

Fig. 2. SEM images, EDAX analysis, and dot mapping analysis for Bare-GCE (**A**, **B**, and **C**), MIL-156 MOF@COF-GCE (**D**, **E**, and **F**), and Au-MIL-156 MOF@COF-GCE (**G**, **H**, and **I**), respectively.

clearly shows the logical reduction of received signals in all 4 techniques which is caused by the non-conductivity feature of antibody and antigen, which prevent the passage of current as a spatial barrier. Considering the different performance of EIS compared to the other three techniques (less current, larger semicircle diameter and vice versa), it can be explained according to Fig. 5B, the diagram (**blue**) shows the largest semicircle with high resistance due to the empty surface of the electrode. Modification of the electrode with MIL156 MOF@COF and Au nanoparticles by electrodeposition, reduced the diameter of the semicircle significantly for the increase in surface area of the electrode and super conductivity of Au (Fig. 4B, **red and green diagrams**). In the next step, by immobilizing the antibody on the modified electrode, the electron transfer resistance increased, which shows that the antibody has covered the surface of the modified electrode as a non-conductive agent (Fig. 5B,

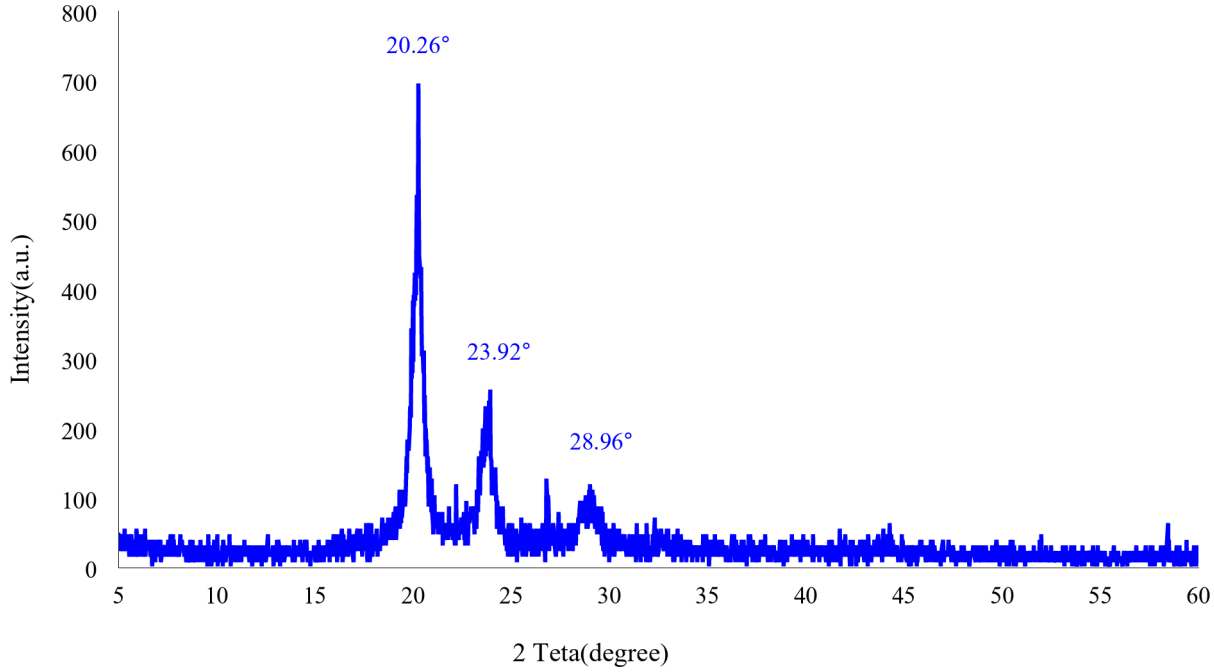

Fig. 3. XRD pattern of MIL-156@COF.

pink diagram). Finally, the proposed biosensor after loading the target antigen, the diameter of the semicircle increased, due to its non-conductivity and blocking the surface, correspondingly (Fig. 5B, **cyan diagram**). The resistance obtained for the modified electrode and the bare electrode was 44.8 and 1787 Ω, respectively. The impressive conductivity of developed nanocomposite compared to the unmodified electrode is evident by measuring the resulting resistance (**Fig. S2**).

Active surface area

Various scan rates, 10-500mV/s were applied and the results are represented in **Fig. S1** for understanding the surface enhancement that is generated after electrode modification with MIL-156@COF@Au. From the **Fig. S1A**, it can be seen that the corresponding peaks of the anode and the cathode currents are rising as the scan rate increases. On the basis, the graph of Ip versus $\upsilon^{1/2}$ was drawn (**Fig. S1B**), in which the slope was determined and from the value of the slope, the modified electrode active surface area was calculated using Randles-Sevcik equation:

$$Ip = 2.69 \times 10^5 \times AD^{1/2} n^{3/2} C \upsilon^{1/2}.$$

D, C, Ip, n, υ and A represents diffusion coefficient, concentration of hexacyanoferrate (5 mM), anodic peak current, number of transferred electron ($n = 1$), scan rate and active surface area of the modified electrode (cm^2), respectively. The area of the modified electrode was calculated as 0. 054 cm^2, which is 72% increase versus the bare electrode.

Calibration

All the parameters are in optimal conditions; different concentrations of CA15-3 antigen were prepared and immobilized on the modified electrode using a dropping strategy and studied in 0.005 M $[Fe(CN)_6]^{3-/4-}$/100 mM KCl solution. According to Fig. 6A and B, the obtained calibration equation is $y = -0.1602x + 39.354$ with a correlation coefficient of $R^2 = 0.9785$, which has established a linear range between the concentrations of 30 and 100 nU/mL, where y and x demonstrated the average peak height and CA15-3 concentration (nU/mL), respectively. For a favorable description, the calibration graph of healthy serum in the presence of different concentrations of CA15-3 antigen is shown, where the equation is $y = -0.2824x + 40.514$ and $R^2 = 0.9841$(Fig. 6C and D). It is discernible from the calibration graph that the slope of the plot related to healthy serum is steeper, and with the increase in antigen concentration, the current dwindles due to other components in healthy serum acting as a non-conducting insulator.

Selectivity

To investigate the proposed biosensor for CA15-3, two potential interferences, including PSA and CA19-9, and the mixed solution of the mentioned two interferences were chosen, respectively, and the interferences were immobilized on the modified electrode and incubated in the refrigerator for half an hour, as same as the calibration curve experiments. It is worth to mention that, the middle point of calibration was chosen as the concentration of the target antigen (CA15-3) for interference studies and the concentrations of the interferers were also diluted to the level of nano units per milliliter. In constant conditions, the prepared biosensor was studied in 0.005 M $[Fe(CN)_6]^{3-/4-}$/100 mM KCl solution to confirm the selectivity. As presented in Fig. 7(**A**

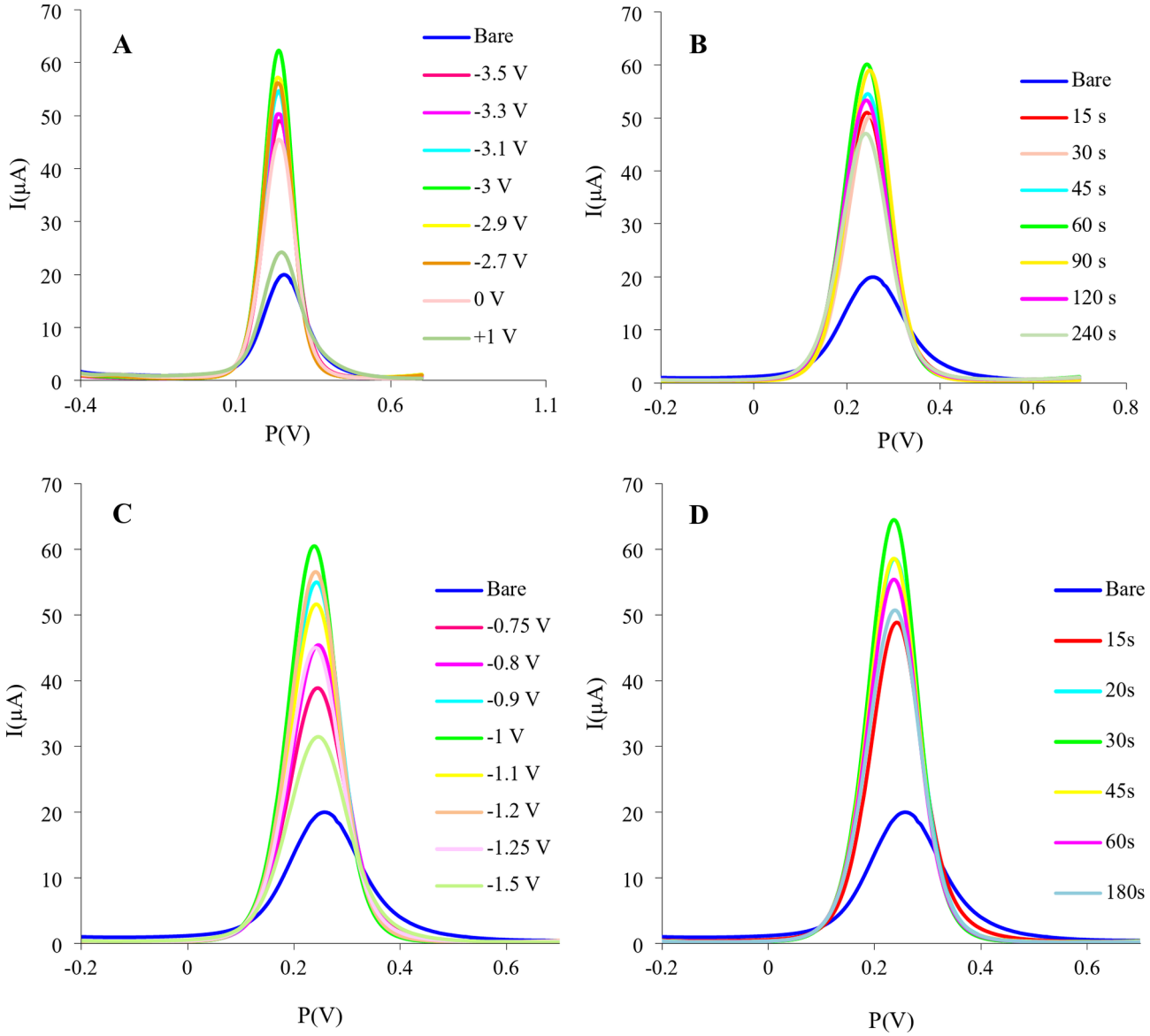

Fig. 4. Electrodeposition of MIL156 MOF@COF with CHA at different deposition potentials (**A**) and times (**B**) and electrodeposition of AuNPs on the modified electrode (MIL156 MOF@COF-GCE) with CHA at different deposition potentials (**C**) and times (**D**) in 0.005 M $[Fe(CN)_6]^{3-/4-}$ a solution containing 100 mM KCl (pH 7.4). Each experiment 5 times repeated ($n = 5$).

and B), the selective biosensor exhibited acceptable selectivity against other biomarkers with minimal cross-reactivity observed.

Repeatability and reproducibility

For the validity of the results, the midpoint of the calibration plot was selected to perform repeatability and reproducibility. For repeatability, the fabricated biosensor with the previously mentioned protocol was measured by the DPV technique and repeated ten times. The relative standard deviation (RSD) for these 10 repeats was calculated to be 1.97%, which indicates a favorable percentage due to the stability of the modifier on the electrode as well as the tight binding between Au and amino groups related to the antibody. To assess the reproducibility of the biosensor, we independently fabricated three separate biosensors using identical protocols. Each biosensor was used to measure the target analyte under the same experimental conditions. Triplicate measurements yielded consistent results across all three fabricated biosensors. The RSD of the measurements was calculated as 1.46%, indicating excellent reproducibility. This low RSD demonstrates the robust and reliable nature of papered biosensor.

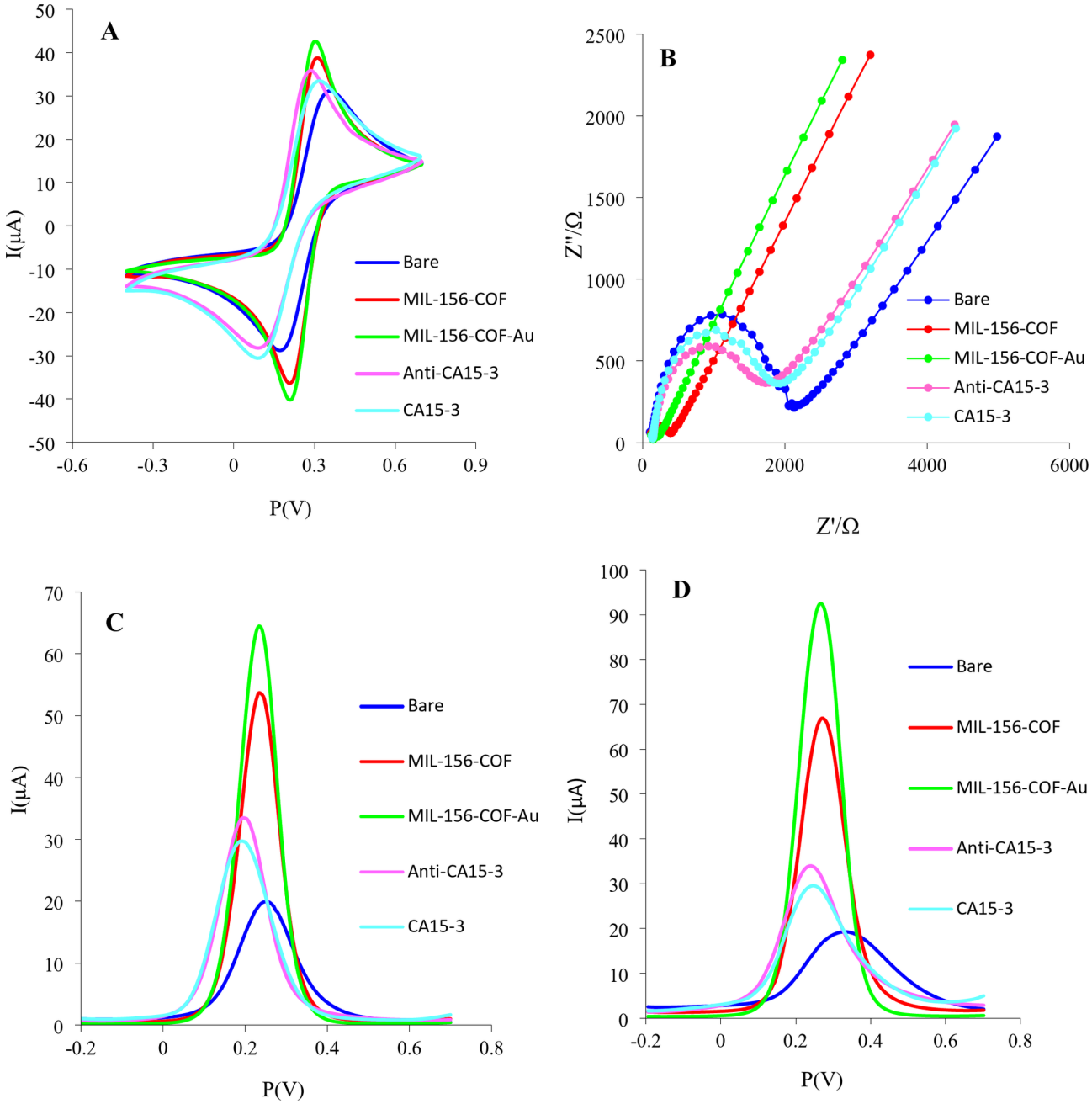

Fig. 5. Description of electrode modification steps. (**A**, **B**, **C** and **D**) are representative of CV, EIS, DPV and SWV methods, respectively.

Clinical sample analysis

To gauge the suggested device in clinical applications, the desired biosensor was evaluated to measure CA15-3 in clinical serum samples (after completing total acquiescence). For this purpose, in optimal conditions according to the mentioned procedures, MIL-156 MOF@COF and Au nanoparticles were respectively electrodeposited on the bare GCE. Next, anti-CA15-3 was immobilized on the modified electrode by covalent bonding to anchor the antigen into a lock-and-key mode. After immobilizing the appropriated amount of human serum on the prepared template, it is incubated for 30 min at 4 °C to determine the concentration of CA15-3 (Fig. 7**(C and D)**). The information obtained from Table 1 shows the massive potential of this biosensor for utilization in the diagnosis of breast cancer suffering patients and also as a points of care device.

Table 1 presents a comparison between the findings of this study and other previously published CA 15 − 3 biosensors. In contrast to previous studies, the nanocomposite used in this work acts as a catalyst for electrochemical activity and improves the overall performance of the fabricated biosensor. The MOF@COF material has both cost-effective and eco-friendly features. It has a distinctive form that allows for a high surface area, making it easier to immobilize a larger quantity of biomolecules. In addition, the significant integration of

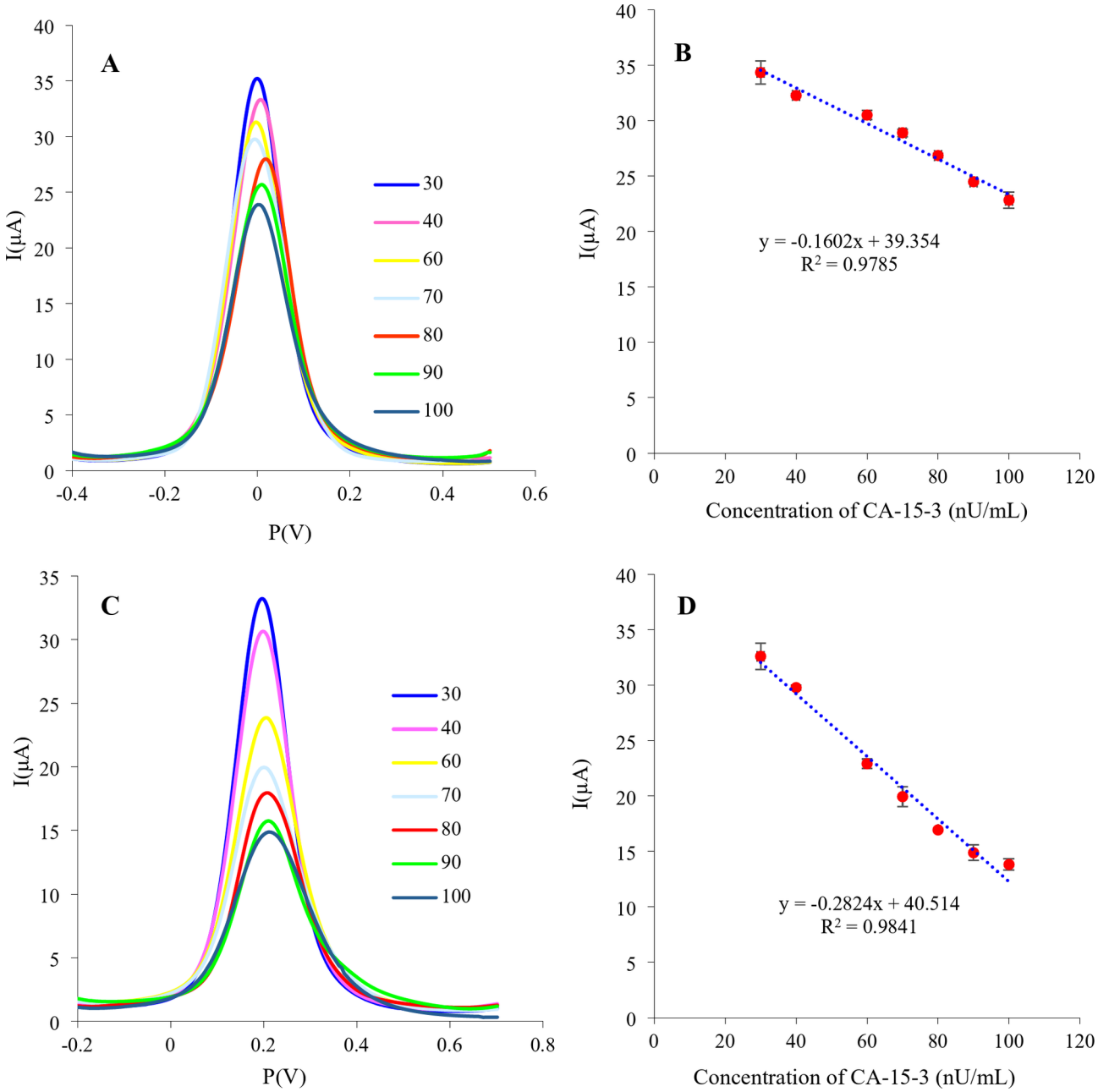

Fig. 6. Concentration effect (from 30 to 100 nu/ mL – CA15-3) on biosensor signals: (**A**) DPV plots and (**B**) Calibration plot of the biosensor. (**C**) and (**D**) calibration plot of the CA15-3 biosensor in the presence of healthy serum. (**C**) The obtained biosensor DPV signals and (**D**) the plotted peak height vs. concentration. Each experiment 5 times repeated ($n = 5$).

biocompatible gold nanoparticles (AuNPs) into the surface of MOF@COF enhances conductivity and provides active sites on the surface. Moreover, the robust bioconjugation between the biotinylated monoclonal CA 15 – 3 antibody and the AuNPs leads to outstanding stability of the designed biosensor. The intrinsic affinity between noble metals and biomolecules guarantees a strong attachment of the biomolecules to the nanocomposite surface, reducing the release of biomolecules and ultimately creating a very stable biosensing platform. In addition, the direct synthesis of core-shell like MOF@COF and the innovative deposition methodology used in this study offer a more efficient strategy in terms of time consuming compared to previous drop casting methods. Furthermore, the utilization of the DPV technique in this study provides improved sensitivity and a lower detection limit, establishing it as an optimal selection for the prompt and precise diagnosis of breast cancer. In addition, the 30 to 100 nU/mL linear detection range and 2.6 nU/mL limit of detection (LOD) are significant achievements, as they allow for the early and sensitive detection of breast cancer biomarkers. The low LOD can be attributed to the combined impact of the nanocomposite's distinct characteristics, the effective bioconjugation, and the precise electrochemical method used.

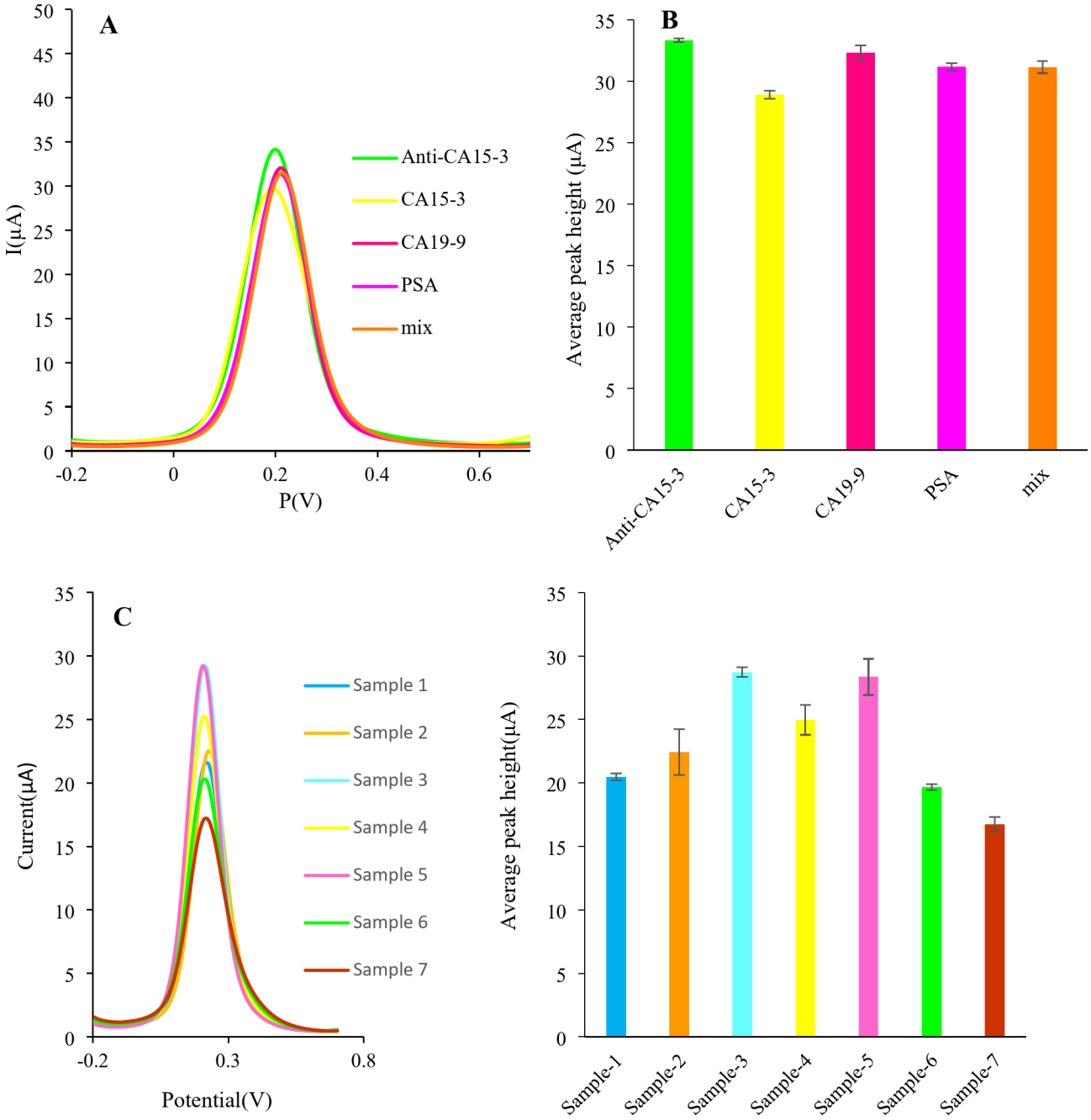

Fig. 7. The specificity of biosensor in the presence of PSA CA-19- 9, and a mixture of them. (**A**) the obtained biosensor DPV plots and (**B**) the corresponded histograms. (**C**) and (**D**) are detection results of CA15-3 with fabricated biosensor in real human serum samples. Each experiment 5 times repeated ($n = 5$).

Conclusion

We designed an EC biosensor based on core-shell MIL-156 MOF@COF nanocomposite decorated with Au nanoparticles to detect CA15-3 protein in human serum samples. The fabricated biosensor supports significant advantages such as high selectivity, good sensitivity, economy, biocompatibility, and simplicity. The presence of core-shell nanocomposite improves the EC signals by increasing the target loading capacity on the bare electrode, and Au nanoparticles, with the tendency to form covalent bonds with anti-CA15-3, provide the biosensor's diagnostic ability as well as its stability. The presented biosensor was used on clinical serum samples to distinguish healthy people from cancerous ones, and the obtained results show this possibility. With these features, the proposed biosensor provides a promising prospect for the immediate and convenient detection of cancer biomarkers and makes new advances in clinical medical research.

Electrode	Detection method	LOD/LLOQ	Linear range	Ref
SPCE/GO/$MoSe_2$/P3ABA/ DAP-AuNPs/CA15-3/BSA/anti-CA15-3	CV, EIS	0.14 U/mL	0-500 U/mL	[49]
GCE Ag/TiO_2/rGO/CA15-3	Amperometry	0.07 U/mL	0.1–300 U/mL	[50]
GCE/Au@Ag NPs/Ab/Ag/Ab/Hg^{2+} SiO_2	DPV, EIS	0.05U/mL	0.1–200 U/mL	[51]
CNE/AuNP/MIP/CA15-3	CV	1.16 U/mL	5–35 U/mL	[52]
GCE/RGO-MoS2/ AuNPs/Apt/BSA/CA15-3	EIS	0.3 U/mL	5-200 U/mL	[53]
Ab2/CQDs-PEI-GO/AuNPs /CA15-3/BSA/Ab1/PDA-AgNPs/GCE	ECL	0.0017 U/mL	0.005-500 U/mL	[54]
GCE/3DGH/AuNPs/Aps/ BSA/CA15-3	DPV	0.112 U/mL	0.01–150 U/mL	[55]
AuSPE/MSA/EDC/Ab/EA	SWV	0.95 U/mL	1-1000 U/mL	[56]
e-PI/Au/Anti-CA15-3	DPV	0.15 U/mL	0.5–200 U/mL	[57]
GE/Strep/mAb/ BSA/ CA15-3	SWV	$15*10^{-6}$ U/mL	$15*10^{-6}$-50 U/mL	[58]
GCE/MIL-156 MOF@COF@Au/CA15-3	DPV	2.6nU/mL	30–100 nU/mL	This work

Table 1. Comparison of the developed biosensor and other different studies for the evaluation of CA15-3 biomarker.

Data availability

"The data will be released by the corresponding author upon responsible request."

Received: 10 June 2024; Accepted: 4 November 2024
Published online: 02 December 2024

References

1. Miller, K. D. et al. Cancer treatment and survivorship statistics, 2016. *Cancer J. Clin.* **66**(4), 271–289 (2016).
2. Lacroix, M. Significance, detection and markers of disseminated breast cancer cells. *Endocr. Relat. Cancer*. **13**(4), 1033–1067 (2006).
3. Paul, S. et al. Epidemiological study on breast cancer associated risk factors and screening practices among women in the holy city of Varanasi, Uttar Pradesh, India. *Asian Pac. J. Cancer Prev.* **16**(18), 8163–8171 (2016).
4. Cifu, G. & Arem, H. Adherence to lifestyle-related cancer prevention guidelines and breast cancer incidence and mortality. *Ann. Epidemiol.* **28**(11), 767–773 (2018). e1.
5. McPherson, K., Steel, C. & Dixon, J. Breast cancer—epidemiology, risk factors, and genetics. *Bmj*. **321**(7261), 624–628 (2000).
6. Shyyan, R. et al. Breast cancer in limited-resource countries: diagnosis and pathology. *Breast J.* **12**, S27–S37 (2006).
7. Nicosia, L. et al. *History of Mammography: Analysis of Breast Imaging Diagnostic Achievements over the last Century. In Healthcare* (MDPI, 2023).
8. Dezhakam, E. et al. *Electrochemical biosensors in exosome analysis; a short journey to the present and future trends in early-stage evaluation of cancers*. Biosensors and Bioelectronics, p. 114980. (2022).
9. Zhang, W. H., Ma, W. & Long, Y. T. Redox-mediated indirect fluorescence immunoassay for the detection of disease biomarkers using dopamine-functionalized quantum dots. *Anal. Chem.* **88**(10), 5131–5136 (2016).
10. Khodashenas, S., Khalili, S. & Forouzandeh Moghadam, M. A cell ELISA based method for exosome detection in diagnostic and therapeutic applications. *Biotechnol. Lett.* **41**, 523–531 (2019).
11. Doldán, X. et al. Electrochemical sandwich immunosensor for determination of exosomes based on surface marker-mediated signal amplification. *Anal. Chem.* **88**(21), 10466–10473 (2016).
12. Zhang, H. et al. Ti3C2 MXenes nanosheets catalyzed highly efficient electrogenerated chemiluminescence biosensor for the detection of exosomes. *Biosens. Bioelectron.* **124**, 184–190 (2019).
13. Wignarajah, S. et al. Colorimetric assay for the detection of typical biomarkers for periodontitis using a magnetic nanoparticle biosensor. *Anal. Chem.* **87**(24), 12161–12168 (2015).
14. Sohrabi, H. et al. *Advances in layered double hydroxide based labels for signal amplification in ultrasensitive electrochemical and optical affinity biosensors of glucose*. Chemosphere, p. 136633. (2022).
15. Sadrabadi, E. A. et al. Alprazolam Detection using an Electrochemical Nanobiosensor based on AuNUs/Fe-Ni@ rGO Nanocomposite. *Biosensors*. **12**(11), 945 (2022).
16. Dezhakam, E. et al. *Electrochemical and optical (bio) sensors for analysis of antibiotic residuals*. *Food Chem.*, p. 138145. (2023).
17. da Silva, E. T. et al. Electrochemical biosensors in point-of-care devices: recent advances and future trends. *ChemElectroChem*. **4**(4), 778–794 (2017).
18. Mohammadpour-Haratbar, A., Zare, Y. & Rhee, K. Y. *Electrochemical biosensors based on polymer nanocomposites for detecting breast cancer: recent progress and future prospects*. *Adv. Colloid Interface Sci.*, p. 102795. (2022).
19. Sohrabi, H. et al. Recent trends in layered double hydroxides based electrochemical and optical (bio) sensors for screening of emerging pharmaceutical compounds. *Environ. Res.* **211**, 113068 (2022).
20. Sadrabadi, E. A. et al. Novel electrochemical biosensor for breast cancer detection, based on a nanocomposite of carbon nanofiber, metal–organic framework, and magnetic graphene oxide. *Bioelectrochemistry*. **155**, 108558 (2024).
21. Gajdosova, V. et al. Electrochemical nanobiosensors for detection of breast cancer biomarkers. *Sensors*. **20**(14), 4022 (2020).
22. Bertok, T. et al. Electrochemical impedance spectroscopy based biosensors: mechanistic principles, analytical examples and challenges towards commercialization for assays of protein cancer biomarkers. *ChemElectroChem*. **6**(4), 989–1003 (2019).
23. Pérez-Fernández, B. & de la Escosura-Muniz, A. Electrochemical biosensors based on nanomaterials for aflatoxins detection: a review (2015–2021). *Anal. Chim. Acta*. **1212**, 339658 (2022).
24. Dezhakam, E. et al. Platinum-perovskite nanocomposite-based Exosensor for specific detection of prostate cancer in clinical settings. *Microchim. Acta*. **191**(10), 593 (2024).
25. Nasrollahpour, H. et al. Nanotechnology-based electrochemical biosensors for monitoring breast cancer biomarkers. *Med. Res. Rev.* **43**(3), 464–569 (2023).
26. Mazloum-Ardakani, M., Amin-Sadrabadi, E. & Khoshroo, A. Enhanced activity for non-enzymatic glucose oxidation on nickel nanostructure supported on PEDOT: PSS. *J. Electroanal. Chem.* **775**, 116–120 (2016).
27. Sadrabadi, E. A. et al. Fabrication of a label-free electrochemical aptasensor to detect cytochrome c in the early stage of cell apoptosis. *Microchim. Acta*. **189**(8), 279 (2022).

28. Azri, F. A. et al. Electrochemical Immunosensor for detection of aflatoxin B1 based on indirect competitive ELISA. *Toxins*. **10**(5), 196 (2018).
29. Mostafa, I. M. et al. Comprehensive review on the electrochemical biosensors of different breast cancer biomarkers. *Sens. Actuators B*. **365**, 131944 (2022).
30. Yuan, R., Li, H. K. & He, H. Recent advances in metal/covalent organic framework-based electrochemical aptasensors for biosensing applications. *Dalton Trans*. **50**(40), 14091–14104 (2021).
31. Sadrabadi, E. A. et al. Sensitive nanobiosensor for miR-155 detection using a novel nanocomposite of carbon nanofiber, metal-organic framework, and two quantum dots. *Microchem. J.* **193**, 109008 (2023).
32. Furukawa, H. et al. The chemistry and applications of metal-organic frameworks. *Science*. **341**(6149), 1230444 (2013).
33. Kreno, L. E. et al. Metal–organic framework materials as chemical sensors. *Chem. Rev.* **112**(2), 1105–1125 (2012).
34. Kökçam-Demir, Ü. et al. Coordinatively unsaturated metal sites (open metal sites) in metal–organic frameworks: design and applications. *Chem. Soc. Rev.* **49**(9), 2751–2798 (2020).
35. Wen, X., Zhang, Q. & Guan, J. Applications of metal–organic framework-derived materials in fuel cells and metal-air batteries. *Coord. Chem. Rev.* **409**, 213214 (2020).
36. Kou, X. et al. Recent advances of covalent organic frameworks and their application in sample preparation of biological analysis. *TRAC Trends Anal. Chem.* **136**, 116182 (2021).
37. Kuehl, V. A. et al. A highly ordered nanoporous, two-dimensional covalent organic framework with modifiable pores, and its application in water purification and ion sieving. *J. Am. Chem. Soc.* **140**(51), 18200–18207 (2018).
38. Wang, S. B. et al. Remodeling extracellular matrix based on functional covalent organic framework to enhance tumor photodynamic therapy. *Biomaterials*. **234**, 119772 (2020).
39. Kandambeth, S., Dey, K. & Banerjee, R. Covalent organic frameworks: chemistry beyond the structure. *J. Am. Chem. Soc.* **141**(5), 1807–1822 (2018).
40. Shahbazi, N., Zare-Dorabei, R. & Naghib, S. M. Design of a ratiometric plasmonic biosensor for herceptin detection in HER2-positive breast cancer. *ACS Biomaterials Sci. Eng.* **8**(2), 871–879 (2022).
41. Hidalgo, T. et al. Crystal structure dependent in vitro antioxidant activity of biocompatible calcium gallate MOFs. *J. Mater. Chem. B*. **5**(15), 2813–2822 (2017).
42. Boyacıoğlu, H. et al. A novel electrochemical kidney injury molecule-1 (KIM-1) immunosensor based covalent organic frameworks-gold nanoparticles composite and porous NiCo2S4@ CeO2 microspheres: the monitoring of acute kidney injury. *Appl. Surf. Sci.* **578**, 152093 (2022).
43. Yan, Y. et al. Facile synthesis of Ti 4+-immobilized Fe 3 O 4@ polydopamine core–shell microspheres for highly selective enrichment of phosphopeptides. *Chem. Commun.* **49**(44), 5055–5057 (2013).
44. Yan, Y. et al. Self-assembling hydrophilic magnetic covalent organic framework nanospheres as a novel matrix for phthalate ester recognition. *ACS Appl. Mater. Interfaces*. **10**(31), 26539–26545 (2018).
45. Gao, C. et al. Facile synthesis of core–shell structured magnetic covalent organic framework composite nanospheres for selective enrichment of peptides with simultaneous exclusion of proteins. *J. Mater. Chem. B*. **5**(36), 7496–7503 (2017).
46. Fathi, A. A. et al. Selective extraction of apixaban from plasma by dispersive solid-phase microextraction using magnetic metal organic framework combined with molecularly imprinted polymer nanocomposite. *J. Sep. Sci.* **46**(17), 2201055 (2023).
47. Ismail, M., Bustam, M. A. & Yeong, Y. F. Gallate-based metal–organic frameworks, a new family of hybrid materials and their applications: a review. *Crystals*. **10**(11), 1006 (2020).
48. Dezhakam, E. et al. Direct profiling of breast cancer-derived extracellular vesicles using Pd-perovskite electrochemical biosensing platform. *Cancer Nanotechnol.* **15**(1), 1–16 (2024).
49. Pothipor, C. et al. A gold nanoparticle-dye/poly (3-aminobenzylamine)/two dimensional MoSe2/graphene oxide electrode towards label-free electrochemical biosensor for simultaneous dual-mode detection of cancer antigen 15 – 3 and microRNA-21. *Colloids Surf., B*. **210**, 112260 (2022).
50. Shawky, A. M. & El-Tohamy, M. Signal amplification strategy of label-free ultrasenstive electrochemical immunosensor based Ternary Ag/TiO2/rGO nanocomposites for detecting breast cancer biomarker CA 15 – 3. *Mater. Chem. Phys.* **272**, 124983 (2021).
51. Li, L. et al. Visual and electrochemical determination of breast cancer marker CA15-3 based on etching of Au@ Ag core/shell nanoparticles. *Int. J. Electrochem. Sci.* **18**(5), 100123 (2023).
52. Oliveira, A. E. F., Pereira, A. C. & Ferreira, L. F. Disposable electropolymerized molecularly imprinted electrochemical sensor for determination of breast cancer biomarker CA 15 – 3 in human serum samples. *Talanta*. **252**, 123819 (2023).
53. Vojgani, Y. et al. Quantitative measurement of CA 15 – 3 cancer biomarker using an electrochemical aptasensor based on the electrodeposition of au thin film on cauliflower-like rGO-MoS2 nanocomposite. *Microchim. Acta*. **190**(10), 406 (2023).
54. Qin, D. et al. A novel carbon quantum dots signal amplification strategy coupled with sandwich electrochemiluminescence immunosensor for the detection of CA15-3 in human serum. *ACS Sens.* **4**(2), 504–512 (2019).
55. Shekari, Z., Zare, H. R. & Falahati, A. Dual assaying of breast cancer biomarkers by using a sandwich–type electrochemical aptasensor based on a gold nanoparticles–3D graphene hydrogel nanocomposite and redox probes labeled aptamers. *Sens. Actuators B*. **332**, 129515 (2021).
56. Rebelo, T. S. et al. Electrochemical Immunosensor for detection of CA 15 – 3 biomarker in point-of-care. *Sens. Bio-Sensing Res.* **33**, 100445 (2021).
57. Hosseinzadeh, L., Fattahi, A. & Khoshroo, A. A flexible paper-based Electrochemical Immunosensor towards Detection of Carbohydrate Antigen 15 – 3. *Anal. Bioanalytical Electrochem.* **14**(5), 445–454 (2022).
58. Nakhjavani, S. A. et al. A highly sensitive and reliable detection of CA15-3 in patient plasma with electrochemical biosensor labeled with magnetic beads. *Biosens. Bioelectron.* **122**, 8–15 (2018).

Acknowledgements

This project was supported by the, Semnan University of Medical Sciences, Semnan, Iran.

Author contributions

"Ehsan Dezhakam and Roya Faraghi Vayghan contributed to all experimental analyses and prepared the draft. Sarina Dehghani and Taha Kafili-Hajlari helped in synthesis and characterization processes. Abdolhossein Naseri supervised the study and participated in the development of the method, and editing. Balal Khalilzadeh supervised the study and participated in the conceptualization, development of the method, and editing. Gulsah Saydan Kanberoglu contributed in data interpreting. Mehdi Dadashpour helped in editing and funding. All authors reviewed the manuscript."

Funding

Semnan University of Medical Sciences (Grant number 3821).

Declarations

Competing interests
The authors declare no competing interests.

Ethics approval and consent to participate
All patients were asked to complete the informed consent. All procedures of this study were approved by the Local Ethics Committee of Semnan University of Medical Sciences (IR.SEMUMS.REC.1402.218). All procedures were done under the declaration of Helsinki.

Consent for publication
Not applicable.

Additional information
Supplementary Information The online version contains supplementary material available at https://doi.org/10.1038/s41598-024-78836-y.

Correspondence and requests for materials should be addressed to A.N., M.D. or B.K.